

# Giant Quantum Electrodynamic Effects on Single SiV Color Centers in Nanosized Diamonds

Malo Bézard, Antton Babaze, Yuliya Mindarava, Rémi Blinder, Valery Aleksandrovich Davydov, Viatcheslav Agafonov, Ruben Esteban, Philippe Tamarat, Javier Aizpurua, Fedor Jelezko, and Brahim Lounis\*



Cite This: *ACS Nano* 2024, 18, 6406–6412



Read Online

ACCESS |



Metrics & More



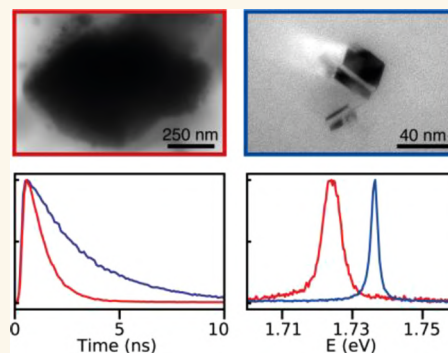
Article Recommendations



Supporting Information

**ABSTRACT:** Understanding and mastering quantum electrodynamics phenomena is essential to the development of quantum nanophotonics applications. While tailoring of the local vacuum field has been widely used to tune the luminescence rate and directionality of a quantum emitter, its impact on their transition energies is barely investigated and exploited. Fluorescent defects in nanosized diamonds constitute an attractive nanophotonic platform to investigate the Lamb shift of an emitter embedded in a dielectric nanostructure with high refractive index. Using spectral and time-resolved optical spectroscopy of single SiV defects, we unveil blue shifts (up to 80 meV) of their emission lines, which are interpreted from model calculations as giant Lamb shifts. Moreover, evidence for a positive correlation between their fluorescence decay rates and emission line widths is observed, as a signature of modifications not only of the photonic local density of states but also of the phononic one, as the nanodiamond size is decreased. Correlative light–electron microscopy of single SiVs and their host nanodiamonds further supports these findings. These results make nanodiamond-SiVs promising as optically driven spin qubits and quantum light sources tunable through nanoscale tailoring of vacuum-field fluctuations.

**KEYWORDS:** silicon-vacancy centers, nanodiamonds, single molecule spectroscopy, quantum electrodynamics, Lamb shift, phonon bottleneck



A quantum emitter interacting with the fluctuations of the electromagnetic vacuum field undergoes spontaneous emission and Lamb shift of its energy levels, which are among the most fundamental effects in quantum electrodynamics.<sup>1</sup> While pioneering studies of these phenomena were performed on atoms in free space, it is now well established that the emission lifetime and the energy shift are impacted by the local electromagnetic environment.<sup>2,3</sup> For instance, engineering the photonic local density of states (LDOS) has been widely used to tune the fluorescence emission rate and directionality of an emitter.<sup>4</sup> Yet, the potential of LDOS engineering on the Lamb shift has been overlooked. Due to the emergence of modern quantum nanophotonic systems, it becomes crucial to accurately predict the energy levels of emitters interacting with tailored vacuum fields. Photonic crystals, consisting of periodic dielectric structures, have been theoretically<sup>5</sup> proposed as candidates to modify the LDOS and induce sub-meV Lamb shifts, which are 1–2 orders of magnitude greater than those achieved in

vacuum.<sup>6</sup> Larger Lamb shifts of several meV are observed for molecules located in the vicinity of plasmonic structures.<sup>7–9</sup> On the other hand, the imaginary part of the permittivity of the metallic structures is responsible for additional nonradiative decay channels that quench the luminescence and significantly broaden the emission lines. Tuning the Lamb shift of an emitter located in the vicinity of dielectric nanostructures has currently been considered not to be competitive with respect to their plasmonic counterparts,<sup>10</sup> and no experimental study has been reported so far. The configuration of an emitter embedded *within* a dielectric structure has only been considered in the context of spontaneous emission.<sup>11,12</sup> Yet,

**Received:** November 24, 2023

**Revised:** February 7, 2024

**Accepted:** February 9, 2024

**Published:** February 14, 2024



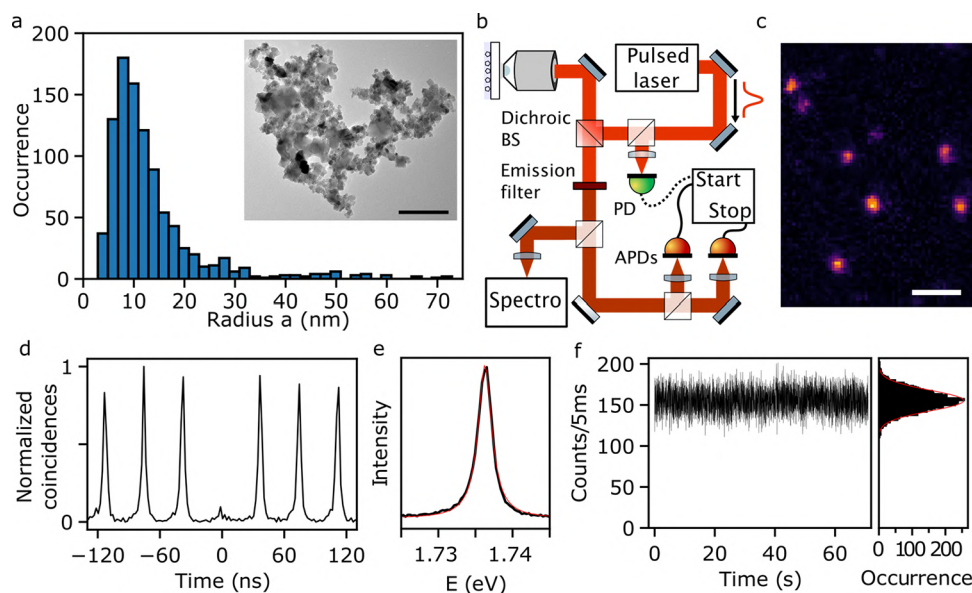


**Figure 1.** (a) Distribution of ND sizes determined by TEM. The batch displays a large dispersion with a 20 nm average diameter. Note that rare microsized ND outliers are still present but not shown here. Inset: Typical high-resolution TEM image of the NDs. Scale bar: 150 nm. (b) Schematics of the experimental confocal setup. The fluorescence is collected via a high numerical aperture objective and separated from the laser illumination with a dichroic beam splitter (BS). Single photons are detected using two avalanche photodiodes (APDs). PD denotes the photodiode used for TCSPC measurements. (c) Typical confocal fluorescence image of NDs containing SiVs. Scale bar: 1  $\mu\text{m}$ . The diffraction-limited spots correspond to single ND emission. (d) The presence of a single emitter in a ND is routinely deduced from an autocorrelation measurement with  $g^{(2)}(\tau = 0) < 0.5$ . (e) Typical fluorescence spectrum (black curve) of a single SiV color center contained in a ND, fitted with a Lorentzian profile (red curve). It displays a sharp ZPL at  $\sim 1.736$  eV with  $\sim 2.2$  meV width. (f) Typical fluorescence time trace (5 ms time resolution) obtained from a single SiV center showing blink-free shot-noise-limited emission. The red curve is the Poisson distribution calculated using the mean counts per time bin.

the local density of photonic states near a dielectric interface, as is the case in nanosized diamonds, provides an attractive nanophotonic platform for strongly modifying vacuum fluctuations to tailor the dynamics and energy of the light emitted by single color centers near the surface. Demonstration of huge Lamb shifts offers the possibility of implementing integrated nanoscale photonic chips, where the photon energy of efficient quantum light sources can be manipulated on demand.

Color centers in diamonds have aroused great interest over the past two decades due to their suitability as quantum light sources and sensors, as well as for single spin manipulation with optical readout in the view of quantum information processing.<sup>13–15</sup> Among them, the negatively charged silicon-vacancy center<sup>16</sup> (SiV) is promising owing to its fluorescence stability in intensity and emission frequency,<sup>17,18</sup> the simplicity of its spin 1/2 ground state, and the dominant proportion of photon emission in the zero-phonon line (ZPL), whose homogeneous width is almost lifetime-limited at low temperature.<sup>19–21</sup> However, in the context of potential use as spin qubits, SiV centers suffer from a short-lived, submicrosecond spin coherence time at cryogenic temperatures above 1 K.<sup>22</sup> Indeed, in this group-IV defect, spin–orbit coupling splits the ground electronic state into a doublet by  $\sim 0.2$  meV (i.e.,  $\sim 50$  GHz),<sup>23,24</sup> which causes efficient coupling of the two fine-structure sublevels to resonant phonon modes<sup>25</sup> that remain populated at these temperatures. Various strategies have been developed to reduce orbital dephasing rates in the SiV ground state, such as using ultralow temperatures  $T \sim 100$  mK<sup>26</sup> or fabricating complex diamond-based nanoelectromechanical structures.<sup>27,28</sup> Since spin relaxations are mediated by acoustic phonons that are strongly influenced by the phonon-mode

density spectrum of the host diamond, the use of ultrasmall nanodiamonds should lead to the suppression of the low-energy phonon modes and thus to reduced orbital thermalization rates.<sup>29</sup>

Here we investigate fundamental quantum electrodynamics effects on individual SiV centers interacting with the vacuum field fluctuations in nanosized diamonds. A large proportion of centers show giant blue Lamb shifts of their emission lines, up to 80 meV with respect to SiV spectra in bulk diamond. These observations are well reproduced by model calculations involving an emission dipole located in a dielectric nanosphere with a high refractive index. These shifts are larger than those produced in analog nanoscale resonators, such as plasmonic nanoantennas.<sup>9</sup> Moreover, combining spectral and time-resolved optical spectroscopy measurements of single SiV defects, we show evidence for a positive correlation between their fluorescence decay rates and their ZPL widths, attributed to correlated modifications in both the photon- and phonon-LDOS as the ND size is decreased. Correlative light–electron microscopy of single SiVs and their host NDs further supports this analysis, which turns SiV-containing nanodiamonds into a versatile nanoscale platform for controlling both the energy and dynamics of the quantum states that cause single photon emission.

## RESULTS AND DISCUSSION

The nanodiamond synthesis and the optical methods used to characterize them are detailed in the **Materials and Methods** section. As shown in **Figure 1a**, most of the particles ( $\sim 95\%$ ) have a radius  $a$  smaller than  $\sim 30$  nm: Their radius distribution is centered on  $a \sim 10$  nm with a full width at half-maximum (fwhm) of  $\sim 9$  nm. A representative transmission electron

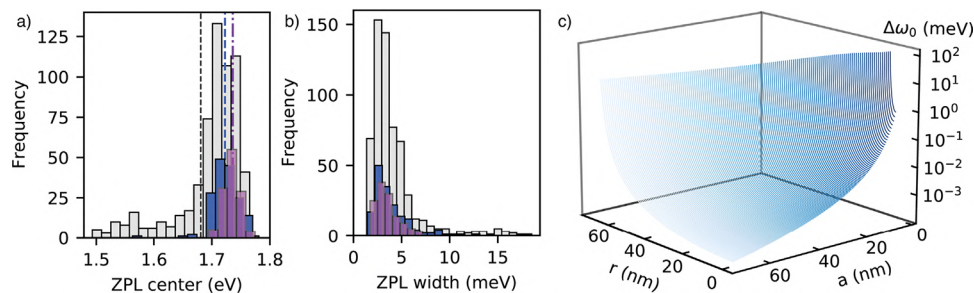


**Figure 2.** Distributions of the ZPL energies (a) and widths (b) for various SiV centers in NDs. The blue and purple histograms are associated with single SiV centers displaying a single emission line, while the gray ones represent the total distributions. The purple histogram was acquired on a high-temperature (425 °C) annealed sample, whereas none was performed for the blue. The medians of single SiV ZPL energies distributions are respectively denoted by the blue dashed and purple dash-dotted lines, respectively blue-shifted by  $\sim 41$  meV and  $\sim 54$  meV from the emission energy in bulk, denoted by the black dashed line. (c) Distribution of the calculated blue shifts, using the classical dipole model, as a function of the ND radius,  $a$ , and the SiV distance,  $r$ , from the center. The shifts are displayed for  $3 < a < 70$  nm,  $0.01a < r < a - 0.357$  nm and  $\theta = 45^\circ$ .

microscopy (TEM) image of the NDs is displayed in the inset of Figure 1a. For single-particle optical studies, the samples are prepared by spin-coating a glass coverslip with a solution of fluorescent NDs in polyvinyl alcohol (PVA), which has an index of refraction close to that of glass ( $\sim 1.48$ ). The coverslip is mounted on an optical setup consisting of a home-built scanning confocal microscope based on a 1.45 numerical aperture immersion oil objective (see Figure 1b). Figure 1c displays a typical confocal image of single NDs recorded by raster scanning the sample with a piezo scanner. Single SiV center emission is then determined using the criterion  $g^{(2)}(0) < 0.5$  as exemplified in Figure 1d, typically displaying a sharp Lorentzian-shaped fluorescence spectrum at room temperature, as advertised in Figure 1e. It was here found to be centered at 1.736 eV (714 nm) with a fwhm of 2.2 meV. Interestingly, more than 80% of single SiV defects exhibit an extremely stable fluorescence signal, with shot noise-limited intensity fluctuations over minutes of acquisition (Figure 1f).

The distributions of ZPL emission energies and widths of SiV defects displaying Lorentzian homogeneous lines are shown in Figure 2a,b. In the histogram plot, the blue and purple distributions correspond to single defects (nonannealed sample in blue, annealed sample in purple), while the gray one is associated with the complete set of encountered centers. Note that fluorescence spots exhibiting  $g^{(2)}(0) > 0.5$  may display spectra with multiple well-resolved Lorentzian ZPLs, which are included in the width and position histograms (gray histograms). The total distribution of emission energies is found significantly blue-shifted ( $\sim 30$  meV) with respect to the bulk-diamond ZPL position at 1.681 eV (black dashed line), and a long red-shifted tail which extends over  $\sim 180$  meV. Strikingly,  $\sim 98\%$  of the single SiV ZPLs (blue histogram) are found to be systematically extremely blue-shifted (up to  $\sim 80$  meV) with a median energy shifted by  $\sim 41$  meV (blue dashed line).

Hydrostatic and uniaxial strain induced by the diamond lattice is commonly introduced to explain the ZPL shifts of ND color centers.<sup>27,30</sup> Supported by DFT calculations, Lindner et al.<sup>30</sup> have found that in NDs, uniaxial strain dominates and can be responsible for large ZPL red shifts up to hundreds of meV, while hydrostatic-type pressure, which are of the order of few GPa,<sup>30</sup> induces limited blue shifts by few meV.<sup>30,31</sup> To explain the large blue shifts observed with their 50–250 nm sized NDs,<sup>30</sup> they suggested that the blue lines may originate from a new class of silicon-based defects. However, the investigated

emission spectra of single defect show that these lines stem from SiV centers. Indeed, we observed that their vibrational features merely resemble those obtained in bulk diamond, where SiV-specific vibrational modes and the  $sp^3$ -linked C–C mode of diamond are clearly identified (cf. section I and Figure S1a in Supporting Information).<sup>23,32,33</sup> Here, we additionally show that the large blue shifts of the transition energies originate from a quantum electrodynamic effect, namely, a giant photonic Lamb shift<sup>4,34</sup> stemming from the interactions of the SiV transition dipole moment with the modified local vacuum field fluctuations in diamond nanostructures. These interactions are strongly enhanced when the dipole is brought close to the dielectric interface, where a strong self-interaction of the transition dipole occurs, an effect more pronounced in small-sized NDs.<sup>35,36</sup>

An estimation of the Lamb shifts can be performed by analyzing the emission of radiation by an emission dipole located inside a diamond nanosphere (of radius  $a$  and refractive index  $n_d = 2.45$ ), at a distance  $r$  from the center and with an orientation angle  $\theta$  from the radial direction. This simplified geometry does not account for crystal facets or sharp edges, which are known to impact the radiative decay rates.<sup>37</sup> The SiV center is considered as a two-level system in the weak coupling regime, for which the quantum calculation of the Lamb shift leads to the same dependence as the classical treatment. Considering the regime of long emission wavelengths with respect to  $a$ , where retardation effects can be neglected, and considering the reaction force acting on the oscillating dipole by the self-interaction electric fields, an analytical expression of the oscillation frequency shift  $\Delta\omega_0$  can be derived:<sup>35</sup>

$$\frac{\Delta\omega_0}{\gamma_b^{\text{rad}}} = \frac{3}{(4\pi c)^3} \frac{n_d^2 - n_e^2}{n_d^3} \frac{\lambda_0^3}{ar^2} \times \sum_{l=0}^{\infty} \frac{l(l+1)}{(n_d^2 + n_e^2)l + n_e^2} \left(\frac{r}{a}\right)^{2l} (l + l \cos^2 \theta + \sin^2 \theta) \quad (1)$$

where  $\gamma_b^{\text{rad}}$  is the SiV dipole radiative decay rate in bulk diamond. Here, we consider a homogeneous external medium whose refractive index  $n_e \approx 1.24$  is the average of air and PVA.<sup>11,38</sup> From eq 1, it is clear that the resulting shifts are to the blue ( $n_d > n_e$ ) and mainly depend on the dipole location  $r$  within the nanoparticle rather than on its orientation  $\theta$ . The

shifts presented in Figure 2c are calculated for various values of  $a$  and  $r$ , for  $\theta = 45^\circ$ . They are found to reach 100 meV for dipoles close (within  $\sim 1$  nm) to the surface of particles with a radius smaller than 100 nm, in agreement with the experimental results. This result is corroborated by a calculation of the photonic Lamb shift obtained from the nonretarded Green's function under such a configuration (see section II of Supporting Information). These quantum electrodynamic corrections also corroborate with the smaller shifts reported by Lindner et al.<sup>30</sup> in the case of larger particles ( $a \sim 35$  nm). Moreover, this effect may also be at the origin of the unexplained strong blue shifts ( $\sim 300$  meV) observed with nitrogen-vacancy centers in ultrasmall ( $a \sim 2.5$  nm) NDs, as reported by Chung et al.<sup>39</sup>

To support this interpretation, we compared the histogram of ZPL positions, measured with NDs embedded in a layer of PVA, to that obtained when NDs were directly spin-coated onto glass without polymer coating and annealed at high temperature (in air for  $\sim 4$  h at  $425^\circ\text{C}$ )<sup>40,41</sup> to remove any onion-like graphitic layer on the NDs surface. Interestingly, we find that the resulting distribution of single-defect ZPL energies (purple histogram in Figure 2a) is even more blue-shifted than previously. Indeed, its median transition energy is shifted by  $\sim 13$  meV with respect to the nonannealed case. This confirms the dependence of the photonic Lamb shift on the dipole location within its ND host, since annealing effectively brings SiV defects closer to the nanoparticle/air interface. This suggests that the local concentration of defects within the NDs volume is nonuniform and increases largely toward the surface.<sup>42</sup> Additionally, to demonstrate the external refractive index dependence, we followed single defect ZPL energies upon controlled modification of the ND dielectric environment (see section III of Supporting Information). To do so, we increase the ND average external refractive index from  $n_{e,1} \approx 1.24$  to  $n_{e,2} \approx 1.5$  by depositing an immersion oil droplet. We observed that, after oil deposition, more than  $\sim 75\%$  of the investigated single-color centers exhibited a decay rate increase and the ZPL red-shift expected from expression 1 (cf. Figure S3 of the Supporting Information). These results are a clear signature of quantum electrodynamic effects on single SiV color centers in nanosized diamonds.

Variations of the host diamond size also affect the photonic LDOS felt by the SiV centers and thus modify their radiative lifetime. For particles with  $a < 100$  nm, the radiative decay rate of the emitter barely depends on its location  $r$  and dipole orientation  $\theta$ . On the other hand, it decreases monotonically with decreasing radii  $a$  toward the zero-size limit value  $\gamma_0^{\text{rad}} = \alpha \gamma_b^{\text{rad}}$  with  $\alpha = 9n_e^5/[n_d(n_d^2 + 2n_e^2)^2]$ <sup>12,35,43</sup> (see section IV of Supporting Information). Given the distribution of ND sizes in our sample (Figure 1a), we expect the radiative decay rates  $\gamma^{\text{rad}}$  of the defects contained in the smallest particles ( $a < 20$  nm) to reach  $\gamma_0^{\text{rad}} \approx 0.14 \gamma_b^{\text{rad}}$  (see Figure S4 of the Supporting Information). The histogram of the fluorescence decay rates measured on single SiVs is displayed in Figure 3. Assuming a particle-independent nonradiative contribution  $\gamma^{\text{nr}}$  to the decay rate  $\Gamma = \gamma^{\text{rad}} + \gamma^{\text{nr}}$ , the broad  $\Gamma$ -distribution provides an indirect signature of a significant radiative yield of SiV centers in bulk diamond. This yield  $\Phi = \gamma_b^{\text{rad}}/\Gamma_b$ , where  $\Gamma_b$  is the total decay rate in bulk diamond, can indeed be estimated from  $\Gamma_b(1 - 0.86\Phi)$ , the expected value for  $\Gamma$  in the small-size limits. The  $\sim 2$ -fold difference (with respect to  $\Gamma_b$ ) observed in the lowest measured decay rates indicates a radiative efficiency of bulk

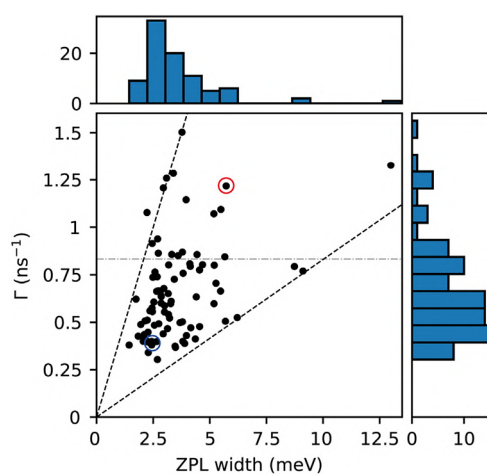


**Figure 3.** Fluorescence decay rate of single SiV centers in NDs is plotted against their ZPL width (fwhm). The horizontal dashed dotted line depicts the SiV total decay rate in the bulk. The dashed lines are guides to the eye to show the correlation between the radiative decay rates and the ZPL widths. Note that the blue and red circles data points relate to the positions of the emitters displayed in Figure 4.

SiV centers as high as  $\sim 60\%$ , in the same order of most recent estimates.<sup>44,45</sup>

Interestingly, a positive correlation is observed in Figure 3 between the ZPL widths of single emitters and their fluorescence decay rates. Since SiVs exhibiting long fluorescence lifetimes are most likely hosted in small NDs, this correlation points to reduced dephasing rates of the optical transition dipole in tiny particles. Indeed, reducing the diamond size down to the nanometric range leads to the suppression of the low-energy acoustic phonons,<sup>46</sup> since only vibration modes with a wavelength smaller than the particle size can develop. From calculations based on the free elastic sphere model, we estimate that the lowest vibrational mode in a 20 nm sized ND has a frequency of  $\sim 400$  GHz. Such modification of the phonon-LDOS reduces the electron–phonon collision probability, which results in lengthening the thermal dephasing time of the optical dipole. Furthermore, since the orbital splitting of the SiV ground state is less than the energy of the lowest acoustic phonon mode, phonon-induced orbital relaxation will be drastically impeded.<sup>25</sup> This explains the remarkably sharp ZPLs observed at room temperature, with widths down to  $\sim 1.3$  meV.

To further support our findings on the major role of size effects on the photophysical properties of SiVs in NDs, we have performed correlative light–electron microscopy and spectroscopy of single defects. For this purpose, the NDs are spin-coated on silicon-nitride window grids with benchmarks, in view of their characterization with wide-field and confocal fluorescence microscopy followed by TEM imaging. Figure 4a shows the superimposed fluorescence and TEM images of a selected region of the sample, while Figure 4b displays a TEM zoom on one of the fluorescence spots attributed to a single SiV center. Similarly, correlated images are displayed in Figure 4c for another region and another single SiV center (Figure 4d). The fluorescence decays and spectra of the two single centers imaged in Figure 4c and Figure 4d are shown in Figure 4e and Figure 4f, respectively. Obviously, the emitter displaying the sharpest ZPL and the longest lifetime is found in the smallest ND. Similar correlations on other particles are

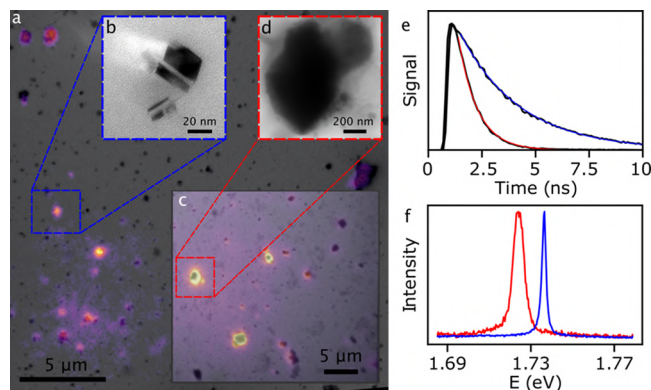


**Figure 4.** Single-defect correlative light-electron microscopy. (a) Superimposed wide-field fluorescence and TEM images of the same region. (b) High-resolution TEM image centered on the single-SiV fluorescence spot framed by the blue dashed square in (a). (c) Similar correlated fluorescence and TEM images of another region, with a TEM zoom (d) on another single SiV fluorescence spot within the red-dashed square. The decay curves and fluorescence spectra on these two single SiV defects are respectively displayed in (e) and (f) with the same color codes. The SiV defect frame in blue (respectively red) has a lifetime of  $\sim 2.5$  ns (respectively  $\sim 0.8$  ns) and a ZPL fwhm of  $\sim 2.3$  meV (respectively  $\sim 5.7$  meV). Note that the optical characteristics of these two defects are represented in Figure 3a with blue and red circles, respectively.

exemplified in section V of Supporting Information. This supports the hypothesis of the host size confinement responsible for modifications of the phonon-LDOS, which lead to a reduction of the orbital dephasing rate of the SiV centers, even at room temperature. Moreover, as illustrated in Figure 4, single SiVs contained in nanodiamonds show significantly blue-shifted emission lines with respect to those in bulk diamond, which further support the presence of giant photonic Lamb shifts.

## CONCLUSION

Single-defect microscopy and spectroscopy investigations show that the photophysical properties of negatively charged SiV centers are intimately linked to the host diamond size. Using small-sized NDs, we unveil unusually large blue shifts in the fluorescence spectra of SiV centers and attribute them to giant photonic Lamb shifts. As these shifts strongly depend on the proximity between the optical dipole and the dielectric interface, they constitute a promising spectroscopic tool to super-resolve the defects' locations at the nanometric scale within small dielectric nanostructures. This work should guide the development of a more quantitative numerical model of photonic Lamb shifts accounting for the ND shape anisotropy such as crystal facets and sharp edges. On the other hand, the observed shifts must be carefully considered in the case of microscopy applications relevant to biology, such as nanoscale multicolor imaging and thermometry.<sup>47,48</sup> Furthermore, lowering the ND size down to the nanometric range leads to a phonon bottleneck effect, which extends the thermal dephasing time of the SiV optical transition dipole and reduces the SiV-spin orbital relaxation, allowing spin coherent manipulation without resorting to millikelvin temperatures.

## MATERIALS AND METHODS

The nanodiamond samples used in this study were obtained by high pressure-high temperature treatment of the catalyst metal-free mixtures of naphthalene with tetrakis(trimethylsilyl)silane and triphenylphosphine (P-doping).<sup>49</sup> This synthesis method allows producing a large fraction of ultrasmall diamond nanoparticles while avoiding a milling step and its inherent damages and stress applied to the particles (cf. Figure 1a). The samples prepared by spin-coating a solution of NDs in PVA are estimated to be embedded in a  $\sim 50$  nm thick polymer matrix layer, using atomic force microscopy. Non-resonant excitation of the NDs is achieved with a focused pulsed laser source (optical parametric oscillator, 150 fs pulse width, repetition rate 80 MHz) at 660 nm. The emitted fluorescence photons are then filtered by a long-pass filter and sent to single-photon detectors or a spectrometer. The fluorescence decay rates of SiV defects are measured with a conventional time-correlated single-photon-counting (TCSPC) setup, while the autocorrelation function  $g^2(\tau)$  of the NDs fluorescence intensity is built using a Hanbury Brown and Twiss coincidence setup.

## ASSOCIATED CONTENT

### Data Availability Statement

Numerical codes used in this study are available from the corresponding author upon request. All data that support the conclusions of this study are included in the article and the Supporting Information file. These data are available from the corresponding author upon request.

### Supporting Information

The Supporting Information is available free of charge at <https://pubs.acs.org/doi/10.1021/acsnano.3c11739>.

Additional information about the numerical evaluation of the Lamb shift, comments about the spatial distribution of defects, and decay rate evolution with size; additional results on the modification of spontaneous emission (emission line and decay rate) upon controlled alteration of the external dielectric environment, as well as correlative light–electron microscopy (PDF)

## AUTHOR INFORMATION

### Corresponding Author

**Brahim Lounis** – *Université de Bordeaux, LP2N, Bordeaux 33405, France; Institut d'Optique and CNRS, LP2N, Bordeaux 33405, France;* [orcid.org/0000-0001-7501-0236](https://orcid.org/0000-0001-7501-0236); Email: [brahim.lounis@u-bordeaux.fr](mailto:brahim.lounis@u-bordeaux.fr)

### Authors

- Malo Bézard** – *Université de Bordeaux, LP2N, Bordeaux 33405, France; Institut d'Optique and CNRS, LP2N, Bordeaux 33405, France;* [orcid.org/0000-0002-5700-6820](https://orcid.org/0000-0002-5700-6820)
- Antton Babaze** – *Materials Physics Center CSIC-UPV/EHU and Donostia International Physics Center DIPC, 20018 Donostia-San Sebastián, Spain;* [orcid.org/0000-0002-9775-062X](https://orcid.org/0000-0002-9775-062X)
- Yuliya Mindarava** – *Institute for Quantum Optics and IQST, Ulm University, Ulm 89081, Germany;* [orcid.org/0000-0003-3668-1672](https://orcid.org/0000-0003-3668-1672)
- Rémi Blinder** – *Institute for Quantum Optics and IQST, Ulm University, Ulm 89081, Germany;* [orcid.org/0000-0001-6655-0150](https://orcid.org/0000-0001-6655-0150)
- Valery Aleksandrovich Davydov** – *L. F. Vereshchagin Institute for High Pressure Physics of RAS, Troitsk 108840 Moscow, Russia*

**Viatcheslav Agafonov** – GREMAN, UMR 7347 CNRS, INSA-CVL, Tours University, Tours 37200, France  
**Ruben Esteban** – Materials Physics Center CSIC-UPV/EHU and Donostia International Physics Center DIPC, 20018 Donostia-San Sebastián, Spain; [orcid.org/0000-0002-9175-2878](https://orcid.org/0000-0002-9175-2878)  
**Philippe Tamarat** – Université de Bordeaux, LP2N, Bordeaux 33405, France; Institut d'Optique and CNRS, LP2N, Bordeaux 33405, France  
**Javier Aizpurua** – Materials Physics Center CSIC-UPV/EHU and Donostia International Physics Center DIPC, 20018 Donostia-San Sebastián, Spain; Ikerbasque, Basque Foundation for Science, 48009 Bilbao, Spain; Department of Electricity and Electronics, University of Basque Country UPV/EHU, 48940 Leioa, Spain; [orcid.org/0000-0002-1444-7589](https://orcid.org/0000-0002-1444-7589)  
**Fedor Jelezko** – Institute for Quantum Optics and IQST, Ulm University, Ulm 89081, Germany

Complete contact information is available at:  
<https://pubs.acs.org/10.1021/acsnano.3c11739>

## Notes

The authors declare no competing financial interest.

## ACKNOWLEDGMENTS

The authors acknowledge M. Ducloy for fruitful discussions. Experiments performed in this work were operated using the Qudi software suite.<sup>50</sup> We acknowledge the financial support from the French National Agency for Research, Région Nouvelle-Aquitaine, Idex Bordeaux (Research Program GPR Light), the EUR Light S&T (PIA3 Program, ANR-17-EUR-0027), and the Laboratory for Transborder Cooperation LTC TRANS-LIGHT from University of Bordeaux and University of the Basque Country. B.L. acknowledges the Institut Universitaire de France. R.E. and J.A. acknowledge financial support from the Basque Government for consolidated groups of the Basque University (Grant IT 1526-22) and MCIN/AEI/10.13039/501100011033/(Grant PID2019-107432GB-I00). We warmly thank E. Gaufres for his help with the high temperature annealing of our samples.

## REFERENCES

(1) Milonni, P. W. *The Quantum Vacuum: An Introduction to Quantum Electrodynamics*; Academic Press, 1994.  
(2) Zhu, S.-Y.; Yang, Y.; Chen, H.; Zheng, H.; Zubairy, M. S. Spontaneous Radiation and Lamb Shift in Three-Dimensional Photonic Crystals. *Phys. Rev. Lett.* **2000**, *84*, 2136–2139.  
(3) Asatryan, A. A.; Botten, L. C.; Nicorovici, N. A.; McPhedran, R. C.; de Sterke, C. M. Frequency shift of sources embedded in finite two-dimensional photonic clusters. *Waves Random Complex Media* **2006**, *16*, 151–165.  
(4) Yao, P.; Van Vlack, C.; Reza, A.; Patterson, M.; Dignam, M. M.; Hughes, S. Ultrahigh Purcell factors and Lamb shifts in slow-light metamaterial waveguides. *Phys. Rev. B* **2009**, *80*, No. 19S106.  
(5) Wang, X.-H.; Kivshar, Y. S.; Gu, B.-Y. Giant Lamb Shift in Photonic Crystals. *Phys. Rev. Lett.* **2004**, *93*, No. 073901.  
(6) Liu, Q.; Song, H.; Wang, W.; Bai, X.; Wang, Y.; Dong, B.; et al. Observation of Lamb shift and modified spontaneous emission dynamics in the YBO<sub>3</sub>:Eu<sup>3+</sup> inverse opal. *Opt. Lett.* **2010**, *35*, 2898.  
(7) Zhang, F.; Yi, J.; Peng, W.; Radjenovic, P. M.; Zhang, H.; Tian, Z.; et al. Elucidating Molecule–Plasmon Interactions in Nanocavities with 2 nm Spatial Resolution and at the Single-Molecule Level. *Angew. Chem-ger Edit* **2019**, *131*, 12261–12265.

(8) Roslowska, A.; Neuman, T.; Doppagne, B.; Borisov, A. G.; Romeo, M.; Scheurer, F.; et al. Mapping Lamb, Stark, and Purcell Effects at a Chromophore-Picocavity Junction with Hyper-Resolved Fluorescence Microscopy. *Phys. Rev. X* **2022**, *12*, No. 011012.  
(9) Zhang, Y.; Meng, Q.-S.; Zhang, L.; Luo, Y.; Yu, Y.-J.; Yang, B.; et al. Sub-nanometre control of the coherent interaction between a single molecule and a plasmonic nanocavity. *Nat. Commun.* **2017**, *8*, 15225.  
(10) Lassalle, E.; Bonod, N.; Durt, T.; Stout, B. Interplay between spontaneous decay rates and Lamb shifts in open photonic systems. *Opt. Lett.* **2018**, *43*, 1950.  
(11) Beveratos, A.; Brouri, R.; Gacoin, T.; Poizat, J.-P.; Grangier, P. Nonclassical radiation from diamond nanocrystals. *Phys. Rev. A* **2001**, *64*, No. 061802.  
(12) Schniepp, H.; Sandoghdar, V. Spontaneous Emission of Europium Ions Embedded in Dielectric Nanospheres. *Phys. Rev. Lett.* **2002**, *89*, No. 257403.  
(13) Ruf, M.; Wan, N. H.; Choi, H.; Englund, D.; Hanson, R. Quantum networks based on color centers in diamond. *J. Appl. Phys.* **2021**, *130*, No. 070901.  
(14) Pompili, M.; Hermans, S. L. N.; Baier, S.; Beukers, H. K. C.; Humphreys, P. C.; Schouten, R. N.; et al. Realization of a multinode quantum network of remote solid-state qubits. *Science* **2021**, *372*, 259–264.  
(15) Sipahigil, A.; Evans, R. E.; Sukachev, D. D.; Burek, M. J.; Borregaard, J.; Bhaskar, M. K.; et al. An integrated diamond nanophotonics platform for quantum-optical networks. *Science* **2016**, *354*, 847–850.  
(16) Becker, J. N.; Neu, E. Chapter Seven The silicon vacancy center in diamond. *Semiconduct Semimet* **2020**, *103*, 201–235.  
(17) Lang, J.; Häußler, S.; Fuhrmann, J.; Waltrich, R.; Laddha, S.; Scharpf, J.; et al. Long optical coherence times of shallow-implanted, negatively charged silicon vacancy centers in diamond. *Appl. Phys. Lett.* **2020**, *116*, No. 064001.  
(18) Bolshedvorskii, S. V.; Zelenev, A. I.; Vorobyov, V. V.; Soshenko, V. V.; Rubinas, O. R.; Zhulikov, L. A.; et al. Single Silicon Vacancy Centers in 10 nm Diamonds for Quantum Information Applications. *ACS Appl. Nano Mater.* **2019**, *2*, 4765–4772.  
(19) Sipahigil, A.; Jahnke, K. D.; Rogers, L. J.; Teraji, T.; Isoya, J.; Zibrov, A. S.; et al. Indistinguishable Photons from Separated Silicon-Vacancy Centers in Diamond. *Phys. Rev. Lett.* **2014**, *113*, No. 113602.  
(20) Neu, E.; Steinmetz, D.; Riedrich-Möller, J.; Gsell, S.; Fischer, M.; Schreck, M.; et al. Single photon emission from silicon-vacancy colour centres in chemical vapour deposition nano-diamonds on iridium. *New J. Phys.* **2011**, *13*, No. 025012.  
(21) Waltrich, R.; Lubotzky, B.; Abudayyeh, H.; Steiger, E. S.; Fehler, K.; Lettner, N.; et al. High-purity single photons obtained with moderate-NA optics from SiV Center in Nanodiamonds on a Bullseye Antenna. *New J. Phys.* **2021**, *23*, 113022.  
(22) Bradac, C.; Gao, W.; Forneris, J.; Trusheim, M. E.; Aharonovich, I. Quantum nanophotonics with group IV defects in diamond. *Nat. Commun.* **2019**, *10*, 5625.  
(23) Rogers, L. J.; Jahnke, K. D.; Doherty, M. W.; Dietrich, A.; McGuinness, L. P.; Müller, C.; et al. Electronic structure of the negatively charged silicon-vacancy center in diamond. *Phys. Rev. B* **2014**, *89*, No. 235101.  
(24) Hepp, C.; Müller, T.; Waselowski, V.; Becker, J. N.; Pingault, B.; Sternschulte, H.; et al. Electronic Structure of the Silicon Vacancy Color Center in Diamond. *Phys. Rev. Lett.* **2014**, *112*, No. 036405.  
(25) Jahnke, K. D.; Sipahigil, A.; Binder, J. M.; Doherty, M. W.; Metsch, M.; Rogers, L. J.; et al. Electron–phonon processes of the silicon-vacancy centre in diamond. *New J. Phys.* **2015**, *17*, No. 043011.  
(26) Sukachev, D. D.; Sipahigil, A.; Nguyen, C. T.; Bhaskar, M. K.; Evans, R. E.; Jelezko, F.; et al. Silicon-Vacancy Spin Qubit in Diamond: A Quantum Memory Exceeding 10 ms with Single-Shot State Readout. *Phys. Rev. Lett.* **2017**, *119*, No. 223602.  
(27) Meesala, S.; Sohn, Y.-I.; Pingault, B.; Shao, L.; Atikian, H. A.; Holzgrafe, J.; et al. Strain engineering of the silicon-vacancy center in diamond. *Phys. Rev. B* **2018**, *97*, No. 205444.

- (28) Sohn, Y.-I.; Meesala, S.; Pingault, B.; Atikian, H. A.; Holzgrafe, J.; Gündoğan, M.; et al. Controlling the coherence of a diamond spin qubit through its strain environment. *Nat. Commun.* **2018**, *9*, 2012.
- (29) Klotz, M.; Fehler, K. G.; Waltrich, R.; Steiger, E. S.; Häußler, S.; Reddy, P.; et al. Prolonged Orbital Relaxation by Locally Modified Phonon Density of States for the SiV- Center in Nanodiamonds. *Phys. Rev. Lett.* **2022**, *128*, No. 153602.
- (30) Lindner, S.; Bommer, A.; Muzha, A.; Krueger, A.; Gines, L.; Mandal, S.; et al. Strongly inhomogeneous distribution of spectral properties of silicon-vacancy color centers in nanodiamonds. *New J. Phys.* **2018**, *20*, No. 115002.
- (31) Vindolet, B.; Adam, M.-P.; Toraille, L.; Chipaux, M.; Hilberer, A.; Dupuy, G.; et al. Optical properties of SiV and GeV color centers in nanodiamonds under hydrostatic pressures up to 180 GPa. *Phys. Rev. B* **2022**, *106*, No. 214109.
- (32) Dietrich, A.; Jahnke, K. D.; Binder, J. M.; Teraji, T.; Isoya, J.; Rogers, L. J.; et al. Isotopically varying spectral features of silicon-vacancy in diamond. *New J. Phys.* **2014**, *16*, No. 113019.
- (33) Ekimov, E. A.; Krivobok, V. S.; Lyapin, S. G.; Sherin, P. S.; Gavva, V. A.; Kondrin, M. V. Anharmonicity effects in impurity-vacancy centers in diamond revealed by isotopic shifts and optical measurements. *Phys. Rev. B* **2017**, *95*, No. 094113.
- (34) Heinzen, D. J.; Feld, M. S. Vacuum Radiative Level Shift and Spontaneous-Emission Linewidth of an Atom in an Optical Resonator. *Phys. Rev. Lett.* **1987**, *59*, 2623–2626.
- (35) Klimov, V. V.; Ducloy, M.; Letokhov, V. S. Spontaneous emission rate and level shift of an atom inside a dielectric microsphere. *J. Mod. Optic* **1996**, *43*, 549–563.
- (36) Barnes, W. L. Fluorescence near interfaces: The role of photonic mode density. *J. Mod. Optic* **1998**, *45*, 661–699.
- (37) Rogobete, L.; Schniepp, H.; Sandoghdar, V.; Henkel, C. Spontaneous emission in nanoscopic dielectric particles. *Opt. Lett.* **2003**, *28*, 1736.
- (38) Ruijgrok, P. V.; Wüest, R.; Rebane, A. A.; Renn, A.; Sandoghdar, V. Spontaneous emission of a nanoscopic emitter in a strongly scattering disordered medium. *Opt Express* **2010**, *18*, 6360.
- (39) Chung, P.-H.; Perevedentseva, E.; Cheng, C.-L. The particle size-dependent photoluminescence of nanodiamonds. *Surf. Sci.* **2007**, *601*, 3866–3870.
- (40) Osswald, S.; Yushin, G.; Mochalin, V.; Kucheyev, S. O.; Gogotsi, Y. Control of sp<sup>2</sup>/sp<sup>3</sup> Carbon Ratio and Surface Chemistry of Nanodiamond Powders by Selective Oxidation in Air. *J. Am. Chem. Soc.* **2006**, *128*, 11635–11642.
- (41) Stehlik, S.; Varga, M.; Ledinsky, M.; Jirasek, V.; Artemenko, A.; Kozak, H.; et al. Size and Purity Control of HPHT Nanodiamonds down to 1 nm. *J. Phys. Chem. C* **2015**, *119*, 27708–27720.
- (42) Plakhotnik, T.; Duka, T.; Davydov, V. A.; Agafonov, V. N. Formation of SiV centers by doping in bottom-up grown HPHT nanodiamonds and its implication for optical nanosensing. *Diam Relat Mater.* **2023**, *139*, No. 110363.
- (43) Chew, H. Radiation and lifetimes of atoms inside dielectric particles. *Phys. Rev. A* **1988**, *38*, 3410–3416.
- (44) Riedrich-Möller, J.; Arend, C.; Pauly, C.; Mücklich, F.; Fischer, M.; Gsell, S.; et al. Deterministic Coupling of a Single Silicon-Vacancy Color Center to a Photonic Crystal Cavity in Diamond. *Nano Lett.* **2014**, *14*, 5281–5287.
- (45) Benedikter, J.; Kaupp, H.; Hümmer, T.; Liang, Y.; Bommer, A.; Becher, C.; et al. Cavity-Enhanced Single-Photon Source Based on the Silicon-Vacancy Center in Diamond. *Phys. Rev. Appl.* **2017**, *7*, No. 024031.
- (46) Albrecht, A.; Retzker, A.; Jelezko, F.; Plenio, M. B. Coupling of nitrogen vacancy centres in nanodiamonds by means of phonons. *New J. Phys.* **2013**, *15*, No. 083014.
- (47) Nguyen, C. T.; Evans, R. E.; Sipahigil, A.; Bhaskar, M. K.; Sukachev, D. D.; Agafonov, V. N.; et al. All-optical nanoscale thermometry with silicon-vacancy centers in diamond. *Appl. Phys. Lett.* **2018**, *112*, No. 203102.
- (48) Liu, W.; Alam, M. N. A.; Liu, Y.; Agafonov, V. N.; Qi, H.; Koynov, K.; et al. Silicon-Vacancy Nanodiamonds as High Perform-
- ance Near-Infrared Emitters for Live-Cell Dual-Color Imaging and Thermometry. *Nano Lett.* **2022**, *22*, 2881–2888.
- (49) Choi, S.; Agafonov, V. N.; Davydov, V. A.; Kulikova, L. F.; Plakhotnik, T. Formation of interstitial silicon defects in Si- and Si,P-doped nanodiamonds and thermal susceptibilities of SiV photoluminescence band. *Nanotechnology* **2020**, *31*, No. 205709.
- (50) Binder, J. M.; Stark, A.; Tomek, N.; Scheuer, J.; Frank, F.; Jahnke, K. D.; et al. Qudi: A modular python suite for experiment control and data processing. *Softwarex* **2017**, *6*, 85–90.